Crystallization, Melting and Morphology of Syndiotactic Polypropylene Fractions. 4. In Situ Lamellar Single Crystal Growth and Melting in Different Sectors

Wensheng Zhou, Stephen Z. D. Cheng,* Sirina Putthanarat, Ronald K. Eby, and Darrell H. Reneker

Maurice Morton Institute and Department of Polymer Science, The University of Akron, Akron, Ohio, 44325-3909

Bernard Lotz

Institute Charles Sadron, 6 Rue Boussingault, Strasbourg 67083, France

Sergei Magonov

Digital Instruments, Santa Barbara, California 93117

Eric T. Hsieh, Rolf G. Geerts, Syriac J. Palackal, Gil R. Hawley, and M. Bruce Welch

Research and Development, Phillips Petroleum Company, Bartlesville, Oklahoma, 74004

Received May 9, 2000; Revised Manuscript Received June 24, 2000

ABSTRACT: Over a wide crystallization temperature (T_c) range, elongated rectangular lamellar single crystals of syndiotactic polypropylene (s-PP) grown from the melt of thin films exhibit sectorization along both diagonal directions to form the (010) [with the (010) free edge] and the (100) [with the (100) free edge] sectors. They can be observed by transmission electron and atomic force microscopy (TEM and AFM). Electron diffraction experiments show that the crystals in both sectors are form III orthorhombic structure, as recently proposed.[1−4] The observation of this sectorization is due to the thickness difference between these two sectors with different fold planes. In situ observations of the single-crystal growth are monitored using an AFM coupled with a hot stage. The T_c-dependent crystal growth rates along both the (100) and (010) normal can be measured, and they are anisotropic. This leads to a large aspect ratio of the rectangular single crystal. AFM results also show that the thickness difference between the two sectors is dependent upon crystallization time (t_c). In the initial stage of single-crystal development, the ratio between the thickness difference and the (100) sector thickness is large [∼35% of the thickness of the (100) thick sectors]. With increasing t_c, this ratio of the thickness difference gradually decreases to ∼15%. Multiple-step cooling and isothermal experiments in a successive T_c-decreasing sequence reveal that each T_c produces a unique lamellar thickness. With reducing T_c, the thickness decreases. Room-temperature TEM observations show that the (010) thin sectors are molten while the (100) thick sectors remain after the single crystals are annealed on a temperature-gradient bar for a prolonged time. In situ single crystal melting monitored by AFM reveals different melting pathways of these two sectors. When the isothermally grown single crystals are heated to 5 °C above T_c (120 °C), the melting first appears in the (100) thick sectors in the form of molten domains. These domains can be repaired via recrystallization if the samples are annealed at this temperature for a long period of time. As further increasing the temperature, the melting of the (100) thick sectors again starts in molten domains along the (100) free edges of the single crystals. In the (010) thin sectors the melting takes place on the free edges of the single crystals, and progresses toward the inner area of the sectors.

Introduction

Since the late 1980s, extensive investigations have been carried out regarding the crystal structure,[1−6] morphology,[1−8] and crystallization and melting[9,10] of syndiotactic polypropylene (s-PP). To briefly summarize, it has been reported that when s-PP is crystallized in the melt, polymorphism can be found. At high crystallization temperatures (T_c), electron diffraction (ED) experiments show that the crystal form possesses an orthorhombic symmetry of *Ibca*, and unit cell dimensions are $a = 1.450$ nm, $b = 1.120$ nm, $c = 0.740$ nm, and $\alpha = \beta = \gamma = 90°$ (form III).[1−4] The chain handedness in the crystal packing is antichiral. The previously reported $C222_1$ orthorhombic unit cell with isochiral chain packing (form I)[11,12] obtained from wide-angle X-ray diffraction (WAXD) experiments in s-PP fibers can only be formed under special deformation treatments[13,14] or at elevated pressures.[15] At relatively low T_c, an orthorhombic unit cell with dimensions identical to form I can be found and its crystal symmetry is $Pca2_1$.[1−4] The handedness of the chain packing in this form is anti- or isochiral along the *b* axis but must be antichiral along the *a* axis. This may be viewed as a slightly disordered state of form III. Several slight modifications of the crystal structures have also been reported.[16−20] Other polymorphisms may also form at even lower T_c, such as the all-*trans*-conformation orthorhombic phase and triclinic intermediate phase.[21]

* To whom correspondence should be addressed. E-mail: cheng@polymer.uakron.edu.

10.1021/ma000802e CCC: $19.00
Published on Web 08/16/2000

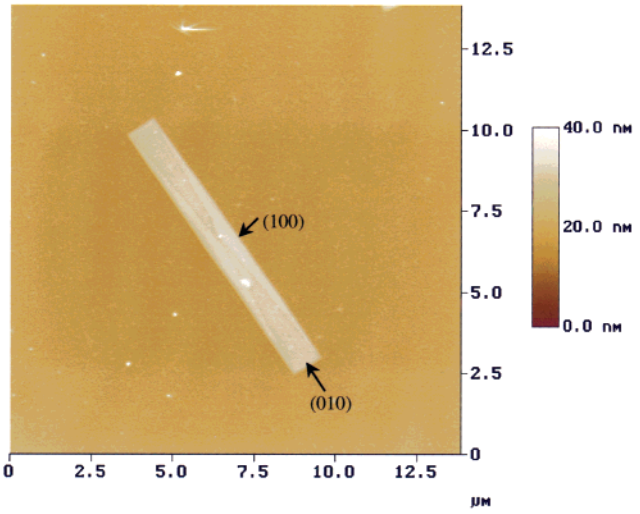

Figure 1. AFM image of a s-PP lamellar single crystal with sectors having two different thicknesses grown from the melt at $T_c = 130$ °C.

Over the past few years, we have reported transmission electron and atomic force microscopy (TEM and AFM) results on sectorization found in s-PP single crystals grown from the melt of thin films.[8] In fact, the sectorization of s-PP single crystals has been shown in even earlier publications.[4,7] The observation of this sectorization under a common TEM-sample preparation procedure is due to a thickness difference between the neighboring sectors in the single crystal.[8] The thick sector is assigned as the (100) sector, since the free edge of the sector is along the (100) plane, while the thin sector is the (010) sector due to the fact that the free edge is along the (010) plane (see Figure 1). There are many important issues remaining unsolved regarding the sectorization. One of them is whether the thickness difference in these two sectors is a true reflection of the variation of the crystal thickness in the single crystal. If it is, the corresponding to thermodynamic stability of the (010) and (100) sectors should be different. The natural deduction is therefore, that the crystal thickness difference is caused either by different crystal structures or different folded surface free energies in these two sectors. On the other hand, it is also possible to imagine that the crystal thicknesses in these sectors are identical, and amorphous layers on the top and bottom of the lamellae are different due to a variation of chain folding behavior.

These speculations must be proven by experimental observations. It is helpful that the formation of sectorization and crystal melting can be monitored in situ in real space to provide advantages in understanding the mechanisms of these processes. In this publication, we focus on investigating the structure and thermodynamic stability of the (100) and (010) sectors using TEM, ED, and AFM techniques. In particular, in situ observations of lamellar single-crystal growth and melting are reported for the first time, using an AFM coupled with a hot stage.

Experimental Section

Materials. The s-PP fractions used were provided by Phillips Petroleum Co., Bartlesville, Oklahoma. A detailed molecular analysis was reported in our previous publications.[8−10] The s-PP fraction used in this study possesses $M_n = 33\,300$, $M_w = 36\,600$, $M_w/M_n = 1.1$, the racemic conformation [r](%) = 94%, the triads [rr](%) = 92%, and the pentads [rrrr] = 86%. Thin film samples were prepared for TEM, ED and AFM experiments. They were cast from solution (in xylene) onto carbon-coated glass slide surfaces, and had thicknesses of around 25−50 nm. The solvent was evaporated at temperatures above the melting temperature (T_m) of s-PP on a hot stage.

Instrumentation and Experiments. Crystal morphology was observed with a TEM (JEOL JEM-1200IIX) with an accelerating voltage of 120 kV. The thin films were isothermally crystallized at different temperatures by heating the samples to 160 °C and holding there for 5 min in a Mettler hot stage (FP-80HT) under a dry nitrogen atmosphere. They were then quickly switched to another Mettler hot stage (FP-90HT), at which an isothermal T_c was preset. After different crystallization times (t_c) in dry nitrogen, the films were cooled rapidly to room temperature. The samples were subjected to a conventional Pt shadowing and carbon backing procedure before being transferred to copper grids for bright field TEM and ED experiments. Calibration of the ED spacing was carried out using TlCl in a *d*-spacing range smaller than 0.384 nm, which is the largest spacing for TlCl. Spacing values greater than 0.384 nm were calibrated by doubling the *d* spacing of those reflections based on the first-order diffraction. To obtain (*hkl*) ED diffractions, a tilting stage was also used.

A temperature-gradient method for melting experiments of the s-PP lamellar single crystals was designed and an apparatus was built using two hot stages, one at either end of a thermally conducting metal bar. These two hot stages were maintained at two different temperatures, such as 130 and 145 °C in dry nitrogen, so that a controlled temperature gradient along the bar was established. At some position along the bar, s-PP lamellar single crystals in the thin films located at a position that had a temperature at which one sector would melt and another section would remain solid if these two sectors possessed two different T_ms.

An AFM (Digital Instrument Nanoscope IIIA) was used to examine the surface topology of the s-PP single crystals under ambient conditions. A 100 μm scanner was selected, and the tapping mode was used to obtain both height and phase images. The force used by the cantilever was light enough to limit damage to the sample, yet heavy enough so that the surface features could be accurately explored. The scanning rate was controlled to be 1−3 Hz for the low magnification images. The data were collected in 512 × 512 pixels per image. Lamellar thicknesses were obtained through scans across the single crystals. An in-house designed hot stage was coupled with the AFM and the temperature range was controlled between 30 and 180 °C. A thermocouple was used to detect the surface temperature of the samples. The temperature variation is generally within ±1 °C.

Results and Discussion

Structure of the Single Crystals in Different Sectors. Figure 1 shows clearly that in an AFM image, sectorization is observed in a lamellar single crystal of s-PP (crystallized at $T_c = 130$ °C). Two sectors can be assigned: the (100) sectors [having the (100) free edge] and the (010) sectors [having the (010) free edge]. For one single crystal, therefore, four sectors are formed and the sector boundary lines are diagonally connected with a crossover at or near the center of the single crystal. The (100) sectors are thicker than the (010) sectors. This shows that at the same T_c, two different thicknesses are found in one s-PP single crystal. The first question that is asked is whether the thickness difference is observed on the bottom of the single lamellar crystal, which is in contact with the carbon-coated substrate. We also grew single crystals on a bare glass slide. The crystals were then detached from the slide and reversed to examine the bottom surface of the crystal. The bottom of the whole crystal is flat and no sectorization can be found. Therefore, the thickness difference between these sec-

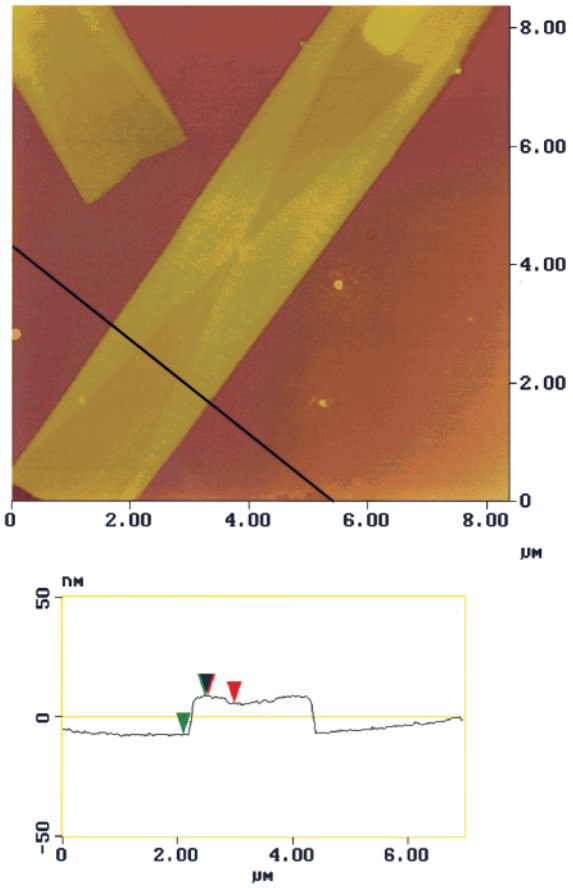

Figure 2. AFM image of a s-PP lamellar single crystal with sectors grown from the melt at $T_c = 130$ °C.

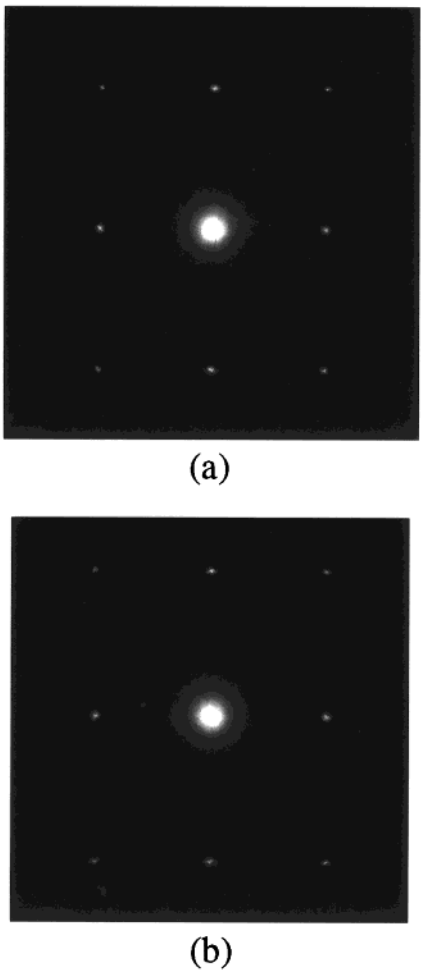

Figure 3. Two ED patterns obtained from each individual sector: (a) in the thicker sector and (b) in the thinner sector.

tors can only exist on the free surface of the lamellar single crystal, and the crystal is asymmetric along the lamellar surface normal direction. This is probably due to growth on a substrate. A quantitative measurement of the thickness difference can be obtained using AFM. Figure 2 shows an AFM morphological profile of a s-PP single crystal (T_c = 130 °C). For this crystal, the thickness of the (100) sectors is 20.6 nm, while that of the (010) sectors is 17.5 nm. The thickness difference between the two sectors is 3.1 nm. The thickness difference ratio, β, which is defined as this difference divided by the thickness of the (100) sector, is ∼15%. Note that the AFM scan across the crystal is carried out at 110 °C in order to clean up the fold surface of the s-PP single crystal by melting the self-decorated polycrystals formed during cooling. We have carried out a number of AFM measurements on the thickness difference between the (010) and the (100) sectors. The ratio β varies between ∼35% and ∼15% of the (100) thick sector. We have also found that this difference is dependent upon both T_c and t_c (see below).

A speculation is that the crystals in the (010) and the (100) sectors may possess different crystal structures. Our ED experimental results in each individual sector show that the [00*l*] zone ED patterns are identical (Figure 3, parts a and b). This suggests that the crystal structure in both sectors is orthorhombic. Note that both forms II and III provide identical [00*l*] zone ED patterns. However, the symmetry of these two forms is different. To identify the exact crystal form in these sectors, tilted ED experiments are carried out. Form III possesses the (211) diffraction when the reciprocal lattice is tilted 42° around the *b** axis, while form II does not have this diffraction. Parts a and b of Figure 4 show ED patterns of the [$\bar{1}$02] zone. The (211) diffraction can be clearly identified for both sectors. This indicates that the crystal structure in both sectors belongs to form III.

In Situ Isothermal Observations of Single-Crystal Growth. It should be noted that all the TEM morphological observations are carried out at room temperature after the s-PP samples were crystallized at a preset T_c for certain period of time, t_c, and then cooled to room temperature. In situ single-crystal growth is monitored at a preset T_c using an AFM coupled with a hot stage. Parts a−d of Figure 5 are a set of successive AFM observations of s-PP single-crystal growth at t_c = 7, 21, 35, and 48 min, respectively, when the s-PP sample is isothermally kept at T_c = 120 °C. Figure 5a shows the sample as crystallized at t_c = 7 min. A small single crystal has been formed on a heterogeneous nucleus (which is most likely an impurity) in the middle part of this figure. Different thicknesses in the (010) and the (100) sectors have been observed even in this stage of crystallization. The dark areas across the middle of the crystal represent the (010) thin sectors and the bright areas are the (100) thick sectors. The length of this single crystal along the (010) normal is about 2.5 μm, and its width along the (100) normal is about 0.25 μm. This leads to an aspect ratio (α) of about 10.0. On the basis of the height results of AFM, the thickness of the (100) thick sectors is 18.5 nm and that of the (010) thin sectors is 12.1 nm. The thickness

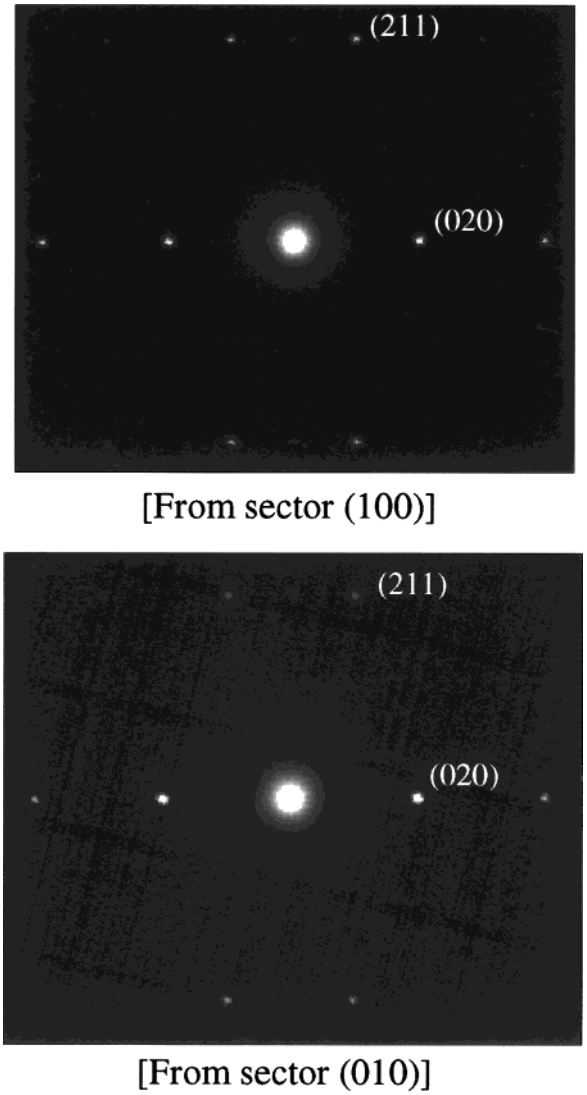

Figure 4. Two 42°-tilted ED patterns obtained from each individual sector: (a) in the thicker sector and (b) in the thinner sector. Both of the ED patterns possess the [102] zone. Note that the (211) diffraction can be clearly seen in both ED patterns.

difference is thus 6.4 nm, which leads to a thickness difference ratio β of ~35%. Assuming that the crystal growth occurs as soon as the temperature reaches 120 °C due to heterogeneous nucleation, the growth rates along both the (010) and (100) normals can be calculated to be $G_{(010)} = (2.5/2)/7 = 0.18$ μm/min and $G_{(100)} = 0.018$ μm/min, respectively. This indicates that the crystal growth rates are highly anisotropic, and the (010) thin sectors grow about 1 order of magnitude faster than the (100) thick sectors.

The growth rate data along the (010) and (100) normal in both the sectors [$G_{(010)}$ and $G_{(100)}$], the lamellar thicknesses in both sectors [$l_{(100)}$ and $l_{(010)}$], the aspect ratios (α) and the thickness difference ratios (β) at t_c = 7, 21, and 35 min are listed in Table 1 for this single crystal. From this table, it is interesting to find that with increasing t_c, the crystal growth rates are almost linear until the single-crystal size becomes large enough. The anisotropic $G_{(010)}$ and $G_{(100)}$ generate an α of ~10. The lamellar crystal thickens in both the sectors. However, the (100) sector thickens in the initial stage of the crystallization and becomes a constant thickness of 20.0 nm at 21 min, while the thin (010) sector continuously thickens even at 35 min. This leads to a decrease of the thickness difference between these two sectors after the single crystal is fully developed, namely, the ratio β gradually decreases from ~35% to ~15% of the thickness of the (100) sectors.

At t_c = 35 min and T_c = 120 °C, as shown in Figure 5c, another lamellar single crystals can be observed and is assigned as B in this figure. Again, this single lamellar crystal possesses a ratio α of 10.0 (a length of 4.7 μm and a width of 0.47 μm). The $G_{(010)}$ is 0.17 μm/min, and the $G_{(100)}$ is 0.016 μm/min. The $l_{(100)}$ is 20.0 nm and the $l_{(010)}$ is 13.0 nm. The ratio β is again ~35%. Note that crystal B is still in a relatively early stage of development.

Further growth of both single crystals A and B at T_c = 120 °C with t_c = 48 min is shown in Figure 5d. Crystal A impinges upon neighboring crystals. This slows the crystal growth rates. However, sectors with different thicknesses are still observed. The ratio β reaches ~15%. On the other hand, crystal B continuously develops to become a crystal with thicknesses and growth rates similar to those of crystal A.

Stepwise cooling experiments for the s-PP crystallization have been carried out as shown in Figure 6, parts a and b. Figure 6a is an AFM height image of a s-PP lamellar single-crystal first crystallized at 130 °C and then quenched to 110 °C for further crystallization. In the center part of this single crystal (indicated by an arrow), which is grown at 130 °C, the $l_{(010)}$ is 17.8 nm. Further overgrowth of this single crystal at 110 °C produces a thinner crystal of that the $l_{(100)}$ is only 10.5 nm. Both regions of the crystals formed at 130 and 110 °C show sectorization. There are also single crystals which only grew at T_c = 110 °C, and observations of thickness show that they are sectorized with a smaller ratio α of 4.2, which is less than half of the original ratio α of the crystals grown at T_c = 130 °C. The $G_{(010)}$ and $G_{(100)}$ are thus less anisotropic than those observed at T_c = 130 °C, revealing that the growth rates along these two directions possess a different T_c dependence. Note that the single-crystal overgrown in the second-step crystallization shows the identical α as that of the single crystal only grown at 100 °C. This indicates that preformed single crystals at 130 °C do not affect the growth behavior of the later developed crystals at T_c = 100 °C.

A four-step temperature decrease (T_c = 115, 95, 85, and 75 °C) with isothermal crystallization at each T_c is shown in Figure 6b (using the phase image) for s-PP thin films observed in AFM. Four different lamellar thicknesses can be found, and each of the thickness corresponds to one isothermal T_c. The thickness measurements indicate that these four $l_{(010)}$s are 13.2, 9.7, 6.1, and 4.1 nm, respectively. Clear boundaries are found for regions grown at each T_c. These observations in parts a and b of Figure 6 illustrate a typical nucleation-controlled crystal growth. Each T_c possesses a kinetically favorable lamellar thickness[22,23] that is not determined by the thickness of the previously formed nuclei.

In Situ Observations of Crystal Melting. A logical question follows: is the overall thickness difference correlated with the difference of crystal thicknesses in these two sectors? Note that thicknesses observed in TEM and AFM include both the crystal thickness and the thickness of the amorphous layers on the top and bottom of lamellar single crystals. There is a possibility

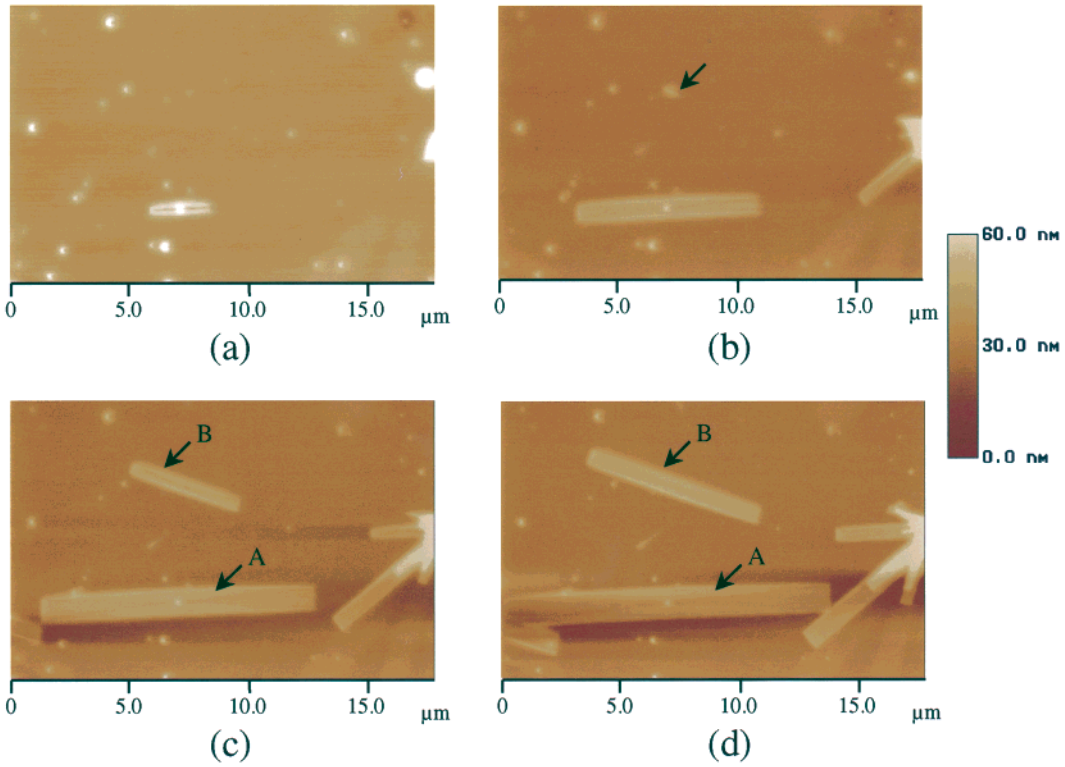

Figure 5. In situ single-crystal growth at 120 °C at different times scanning using AFM (the high images): (a) t_c = 7 min; (b) 21 min; (c) 35 min; (d) 48 min.

Table 1. Growth Rates [$G_{(010)}$ and $G_{(100)}$], Lamellar Thicknesses [$l_{(100)}$ and $l_{(010)}$], Aspect Ratios (α), and Ratio of the Thickness Difference Compared with the Thickness of the (100) Sectors (β) of a s-PP Single Lamellar Crystal A for Different t_cs at T_c = 120 °C

t_c (min)	$G_{(010)}$ (μm/min)	$G_{(100)}$ (μm/min)	$l_{(100)}$ (nm)	$l_{(010)}$ (nm)	α	β
7	0.18	0.018	18.5	12.1	10.0	35%
21	0.18	0.017	20.0	13.2	10.3	35%
35	0.14	0.013	20.0	16.7	10.3	16%

that the thickness difference between these two sectors is caused by a variation of the amorphous layers rather than the crystal thickness. To resolve this issue, we used the temperature-gradient method to perform melting experiments with the sectorized s-PP single crystals. If the crystal thickness in both sectors is not identical, their T_ms must be different. Therefore, it should be possible to melt one sector and retain the other. Figure 7a shows a sectorized s-PP lamellar crystal (T_c = 130 °C) after the sample was kept on the temperature-gradient bar in the melting experiments for a prolonged time. It is evident that the (010) sector partially melts while the (100) sectors remain in the crystal form. Furthermore, it is interesting that the melting of the (010) sector stops as soon as thicker lamellar crystals are formed along both the sides of the boundaries between crystalline and melted materials via a recrystallization/reorganization process. Therefore, the rest of the crystals in the (010) sector behind the just developed thicker lamellae cannot be further melted due to the restriction of the two-dimensional space in the (010) sectors. This bit of thin crystal is thus confined and becomes a superheated metastable crystal.[24−26] A necessary condition for this phenomenon to occur should be that the *b*/4 shift defect accumulations[4] do not occur in the (010) sectors, and therefore, no empty spaces are available for a volume expansion due to the melting. The ED pattern shown in the insert of Figure 7a indicates that the crystal structure, after the partial melting, does not change. The (010) sector can also be completely molten as shown in Figure 7b. This is due to the fact that the thin film sample is located at a slightly higher temperature on the temperature-gradient bar and the (010) sector melting is fast enough to prevent the formation of thicker lamellar crystals.

Note that TEM observations are carried out at room temperature after the s-PP samples are kept on the temperature-gradient bar for a prolonged period of time. It is highly desirable to monitor the in situ melting process of the s-PP lamellar single crystals. Using the AFM coupled with the hot stage, we start from the lamellar single crystals of Figure 5d, shown again in Figure 8a, which were isothermally crystallized at 120 °C for 48 min. We then heated the sample to 125 °C, which is 5 °C higher than the T_c. It is surprising that the majority of crystal melting occurs in the (100) thick sectors as shown in Figure 8b. The melting starts from parts along the long edges of the (100) sectors to form melting domains in both single crystals A and B. After the crystals have been held isothermally at 125 °C for 26 min, the molten domains repair themselves to form perfect linear edges as shown in Figure 8c. When the sample is further heated to 127 °C, as shown in Figure 8d, both the (010) sectors and the (100) sectors start to melt. The molten domains in the (100) sectors are obvious, while the (010) sectors initially melt on the (010) edges, and the melting gradually progresses toward the center of the sectors. Most interestingly, the molten domains formed at 127 °C in Figure 8d are not at the same locations as those of the previously formed molten domains at 125 °C in Figure 8b. This indicates that the repaired domains at 125 °C in Figure 8c possess an improved thermodynamic stability. If we stay at this temperature long enough (e.g., a few hours), the (010)

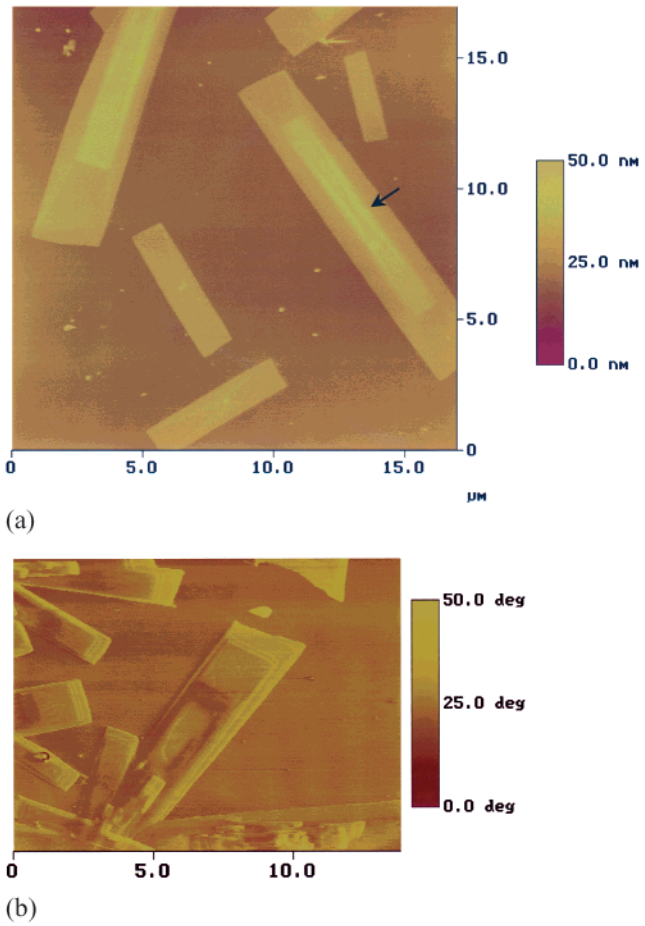

Figure 6. AFM height image of a two-step isothermal crystallization experiment at T_c = 130 and 110 °C for a s-PP sample (a); four-step isothermal crystallization experiment at T_c = 115, 95, 85, and 75 °C for a s-PP sample (phase images) (b).

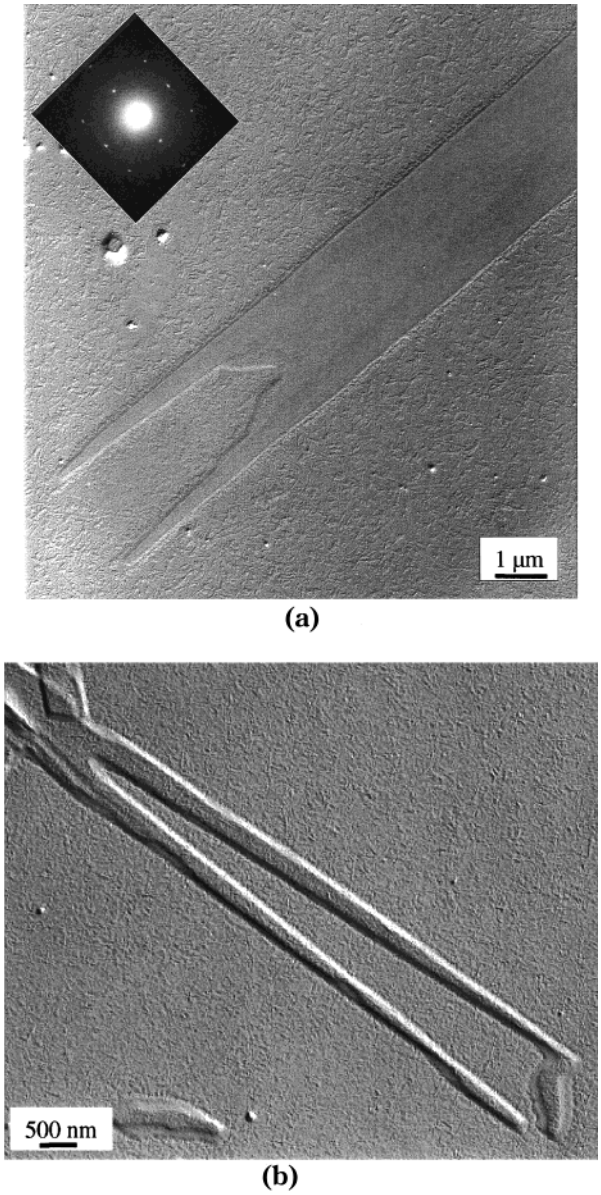

Figure 7. Partially molten (010) sector of a s-PP lamellar single crystal (T_c = 130 °C) observed in TEM using the temperature-gradient melting method. Note that the thicker crystal grown along the crystal/melting boundary in the (010) sector stops further melting of the crystals in the (010) sector (a). (b) a completely molten (010) sector of a s-PP lamellar single crystal (T_c = 135 °C).

sectors can again be repaired. Nevertheless, the (100) sectors cannot be recovered. Therefore, the TEM observations in Figure 7, parts a and b, are the results of the (100) sectors in the crystals having partially melted and then repaired themselves to achieve a higher stability while the sample was kept on the temperature-gradient bar for more than 10 hours. An interesting note is when the AFM was used to examine the height profile of the remaining single crystals as shown in Figures 7b and 8d, the molten s-PP molecules in the (010) sectors have collapsed into melted thin films, which have a height similar to that of the surroundings.

The explanation of this in situ experimental observation is our next step. The molten domains must be closely associated with defects accumulated in the (100) sectors of single crystals. As reported previously, the defects in s-PP single crystals formed at high T_cs consist of individual rows of chains displaced by a b/4 shift of the chain packing along the b axis direction, while at low T_cs, entire groups of such chains are displaced by b/4 forming discrete domains.[4] In the single crystals as discussed here, the b/4 displacements of the chains along the long edge of the crystals must occur in the (100) sectors. Note that the chain folding direction in the (100) sectors is along the b axis.[4,8] This suggests that in these sectors, there are defects accumulated in certain locations, which possess relatively high free energies that destabilize the crystals and provide nuclei for the crystal melting. The observations of the molten domains that developed from points along the free edges of the (100) sectors in Figure 8, parts b and d, may represent the locations of defect accumulations.

The (010) sectors do not exhibit this melting domain phenomenon. One of the possible explanations is that since the chain folding in this sector is most likely along the (110) planes,[8] the lateral growth front of the (010) planes has a zigzag shape on the molecular packing scale. A newly attached chain stem on the zigzag growth front may not substantially increase the lateral surface free energy, and the growth rate along the (010) normal direction is thus fast. This type of crystal growth may have little possibility in accumulating the b/4 displacement as defects that provide nuclei for melting. The question of why the thicknesses of these two sectors are different still remains. The most probable explanation at this moment is due to varying chain folding behaviors in these two different sectors, which leads to different

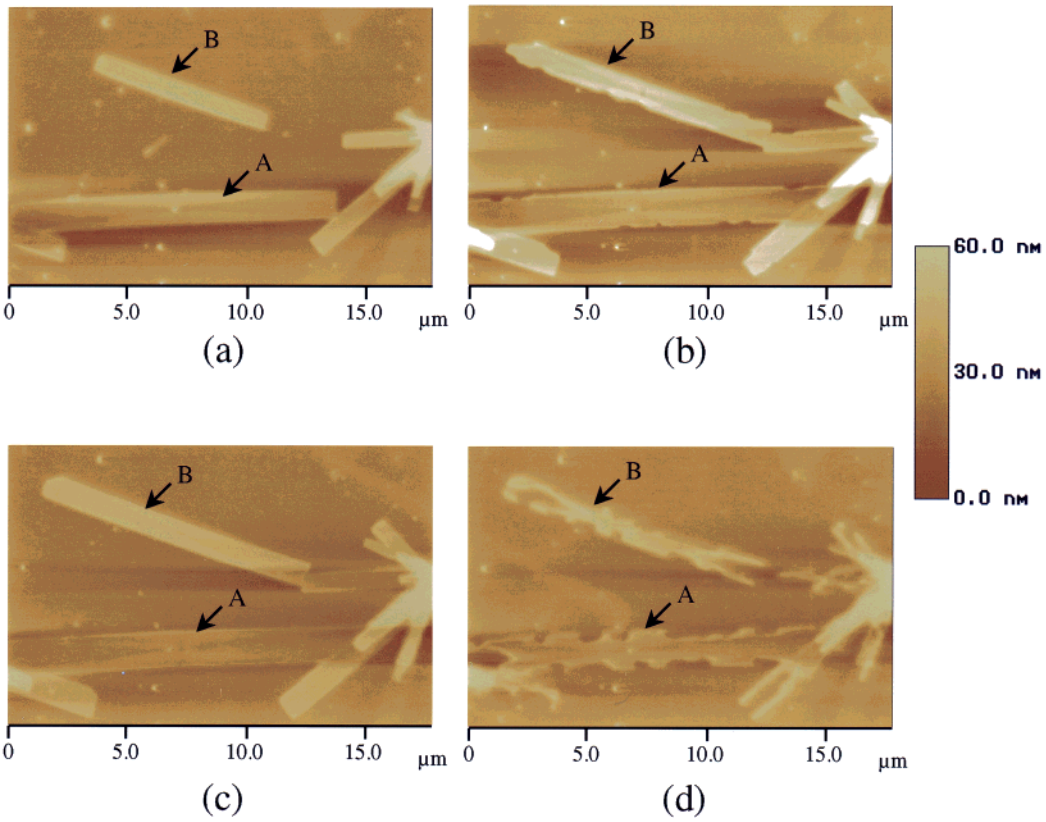

Figure 8. In situ single-crystal melting observed by AFM (height images) after the sample was crystallized at 120 °C: (a) same sample as in Figure 5d; (b) sample heated to 125 °C; (c) sample after annealing at 125 °C for 26 min; (d) sample heated to 127 °C.

folded surface free energies. Further investigation is necessary to achieve a complete understanding.

Conclusion

In summary, we have shown that in s-PP lamellar single crystals, sectorization exists with different thicknesses in the (100) and (010) sectors, and both sectors possess the same crystal structure of form III based on the ED results. In situ single-crystal growth can be observed using an AFM coupled with a hot stage. At T_c = 120 °C, the growth rate $G_{(010)}$ is about 1 order of magnitude faster than $G_{(100)}$, leading to a large aspect ratio α of the single crystals. The sectorization occurs at the beginning of the single-crystal growth, which is associated with different lamellar thickness. The thickness of both sectors increases during the isothermal crystallization. After the $l_{(100)}$ stops thickening, the $l_{(010)}$ continues to increase. This leads to a decrease of the thickness difference ratio β from ∼35% in the initial stage to ∼15% in the later stage of crystallization. Stepwise cooling experiments for crystallization exhibit multiple lamellar thicknesses of the single crystals, revealing the thickness dependence on T_c (or, more precisely, the undercooling). The thermodynamic stabilities of these two sectors are found to be different for the perfectly annealed crystals: the (010) thin sectors apparently melt at a lower temperature compared with the (100) thick sectors observed in TEM. Superheated thinner crystals in the (010) sectors can be observed as soon as they are confined by the thicker lamellar crystals surrounding them. However, in the AFM observations of in situ crystal melting, after heating the single crystals to only 5 °C above the T_c (120 °C), the (100) thick sectors start to melt along the free edges at the domains where defects have accumulated and served as melting nuclei. These molten domains can be repaired via a recrystallization process while annealing at this high temperature for an extended period of time. Further heating the single crystals leads to a melting of both sectors along different melting pathways. For the thick (100) sectors the melting again takes place via melting domains, while in the thin (010) sectors, the melting process starts on the (010) free edges and progresses toward the inside of the sectors.

Acknowledgment. This work was supported by the NSF (DMR-9617030) and Phillips Petroleum Co.

References and Notes

(1) Lotz, B.; Lovinger, A. J.; Cais, R. E. *Macromolecules* **1988**, *21*, 2375.
(2) Lovinger, A. J.; Lotz, B.; Davis, D. D. *Polymer* **1990**, *31*, 2253.
(3) Lovinger, A. J.; Davis, D. D.; Lotz, B. *Macromolecules* **1991**, *24*, 552.
(4) Lovinger, A. J.; Lotz, B.; Davis, D. D.; Padden, F. J., Jr. *Macromolecules* **1993**, *26*, 3494.
(5) Lovinger, A. J.; Lotz, B.; Davis, D. D.; Schumacher, M. *Macromolecules* **1994**, *27*, 6603.
(6) Lotz, B.; Mathieu, C. Thierry, A.; Lovinger, A. J.; De Rosa, C. Ruiz de Ballesteros, O.; Auriemma, A. *Macromolecules* **1998**, *31*, 9253.
(7) Tsukruk, V. V.; Reneker, D. H. *Macromolecules* **1995**, *28*, 1370.
(8) Bu, Z.; Yoon, Y.; Ho, R.-M.; Zhou, W.; Jangchud, I. Eby, R. K.; Cheng, S. Z. D. Eric, T. Hsieh, E. T.; Johnson, T. W.; Geerts, R. G.; Palackal, S. J.; Hawley, G. R.; Welch, M. B. *Macromolecules* **1996**, *29*, 6575.
(9) Rodriguez-Arnold, J.; Zhang, A.; Cheng, S. Z. D.; Lovinger, A. J.; Hsieh, E. T.; Chu, P.; Johnson, T. W.; Honnell, K. G.; Geerts, R. G. Palackal, S. J.; Hawley, G. R.; Welch, B. *Polymer* **1994**, *35*, 1884.

(10) Rodriguez-Arnold, J.; Bu, Z.; Cheng, S. Z. D.; Hsieh, E. T.; Johnson, T. W.; Geerts, R. G. Palackal, S. J.; Hawley, G. R.; Welch, B. *Polymer* **1994**, *35*, 5194.
(11) Natta, G.; Pasquon, I.; Corradini, P.; Perdldo, M.; Pegoraro, M.; Zambelli, A. *Rend. Accad. Naz. Lincei.* **1960**, *28*, 541.
(12) Corradini, P.; Natta, G.; Ganis, P.; Temussi, P. *J. Polym. Sci., Part C* **1967**, *16*, 2477.
(13) De Rosa, C.; Corradini, P. *Macromolecules* **1993**, *26*, 5711.
(14) De Rosa, C.; Auriemma, F.; Vinti, V. *Macromolecules* **1998**, *31*, 7430.
(15) Rastogi, S.; Loos, J.; Cheng, S. Z. D.; Lemstra, P. J. *Polym. Mater. Sci. Eng*, *ACS* **1999**, *218*, 153.
(16) Auriemma, F.; De Rosa, C.; Corradini, P. *Macromolecules* **1993**, *26*, 5719.
(17) De Rosa, C.; Auriemma, F.; Corradini, P. *Macromolecules* **1996**, *29*, 7452.
(18) Lacks, D. J. *Macromolecules* **1996**, *29*, 1849.
(19) Palmo, K.; Krimm, S. *Macromolecules* **1996**, *29*, 8549.
(20) De Rosa, C.; Auriemma, F.; Vinti, V. *Macromolecules* **1997**, *30*, 4137.
(21) See a recent review, for example: Rodriguez-Arnold, J.; Bu, Z.; Cheng, S. Z. D. *J. Macromol. Sci.—Rev. Macromol. Chem. Phys.* **1995**, *C35*, 117.
(22) Hoffman, J. D.; Davis, G. T.; Lauritzen, J. I., Jr. In *Treatise on Solid State Chemistry*; Hannay, N. B., Ed.; Plenum: New York, 1976; Vol. 3, Chapter 7, pp 497−614.
(23) Hoffman, J. D.; Miller, R. L. *Polymer* **1997**, *38*, 3151.
(24) Kovacs, A. J.; Straupe, C.; Gonthier, A. *J. Polym. Sci., Polym. Symp.* **1977**, *59*, 31.
(25) Keller, A.; Cheng, S. Z. D. *Polymer* **1998**, *39*, 4461.
(26) Cheng, S. Z. D.; Keller, A. *Annu. Rev. Mater. Sci.* **1998**, *28*, 533.

MA000802E